ACS OMEGA

Open Access

http://pubs.acs.org/journal/acsodf

Article

Cerium Oxide Nanozymes Improve Skeletal Muscle Function in Gestational Diabetic Offspring by Attenuating Mitochondrial Oxidative Stress

Xinyuan Li, Wanbo Zhu, Rui Liu, Guolian Ding,* and Hefeng Huang*

Cite This: *ACS Omega* 2024, 9, 21851−21863

Read Online

ACCESS | Metrics & More | Article Recommendations | Supporting Information

ABSTRACT: Gestational diabetes mellitus (GDM) is a significant complication during pregnancy that results in abnormalities in the function of multiple systems in the offspring, which include skeletal muscle dysfunction and reduced systemic metabolic capacity. One of the primary causes behind this intergenerational effect is the presence of mitochondrial dysfunction and oxidative stress in the skeletal muscle of the offspring due to exposure to a high-glucose environment in utero. Cerium oxide (CeO_2) nanozymes are antioxidant agents with polymerase activity that have been widely used in the treatment of inflammatory and aging diseases. In this study, we synthesized ultrasmall particle size CeO_2 nanozymes and applied them in GDM mouse offspring. The CeO_2 nanozymes demonstrated an ability to increase insulin sensitivity and enhance skeletal muscle motility in GDM offspring by improving mitochondrial activity, increasing mitochondrial ATP synthesis function, and restoring abnormal mitochondrial morphology. Furthermore, at the cellular level, CeO_2 nanozymes could ameliorate metabolic dysregulation and decrease cell differentiation in adult muscle cells induced by hyperglycemic stimuli. This was achieved through the elimination of endogenous reactive oxygen species (ROS) and an improvement in mitochondrial oxidative respiration function. In conclusion, CeO_2 nanozymes play a crucial role in preserving muscle function and maintaining the metabolic stability of organisms. Consequently, they serve to reverse the negative effects of GDM on skeletal muscle physiology in the offspring.

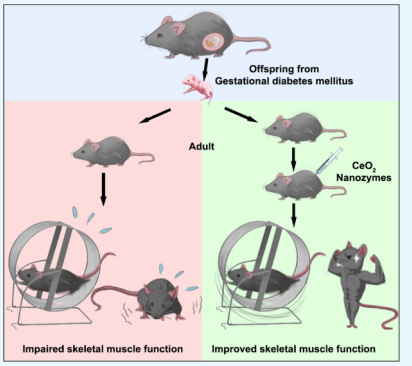

1. INTRODUCTION

Gestational diabetes mellitus (GDM) is one of the most common pregnancy complications, affecting up to 15% of pregnant females worldwide.[1] The offspring born to mothers with GDM often experience serious complications, such as stillbirth, neonatal death, macrosomia, and neonatal respiratory distress. In addition to these short-term effects, these offspring also face numerous long-term health risks. Studies have reported that the offspring exposed to hyperglycemia in utero have a significantly increased risk of adiposity, metabolic diseases, impaired neuromuscular development, and cardiovascular dysfunction in adulthood.[2,3] Several studies have demonstrated that impaired skeletal muscle function, including metabolic sensitivity and mitochondrial dysfunction, is a major manifestation in offspring exposed to maternal overnutrition.[4] These adverse effects are primarily caused by excessive oxidative stress and inflammation induced by the hyperglycemic environment in the mother.[5] Mitochondrial respiratory function is highly susceptible to external oxidative stress. Stimulation from a high glucose environment can exacerbate inflammation and oxygen-free radical levels, leading to damage to mitochondrial function. Given that metabolic and inflammatory symptoms in GDM offspring are typically at a subclinical stage, the use of potent anti-inflammatory and antioxidant drugs is currently not recommended for this population.

The rise of nanozymes holds promise for sustainably renewable and low-toxicity antioxidant treatments.[6] Among the most representative nanozymes, cerium oxide (CeO_2) nanozymes have attracted significant attention due to their typical nanozymatic activity, low toxicity, and the ability to easily adjust their electronic configurations in response to changes in the biological environment.[7] CeO_2 nanoparticles (CNPs) contain ions in two oxidation states (Ce^{3+} and Ce^{4+}) on their surface, and the presence of highly mobile oxygen vacancies in the lattice enables these cerium ions to freely alternate their oxidation states in a reversible manner.[8] This redox change allows each active site in the CeO_2 nanozyme structure to interact with and convert multiple reactive oxygen species (ROS) molecules into inert molecules, resulting in a variety of antioxidant enzyme-like activities, including superoxide dismutase (SOD), catalase (CAT), and peroxidase-like activities.[9] Under suitable conditions, CeO_2 nanozymes can scavenge almost all types of harmful active substances, outperforming

Received: November 13, 2023
Revised: April 14, 2024
Accepted: April 30, 2024
Published: May 10, 2024

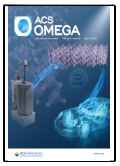

https://doi.org/10.1021/acsomega.3c09025
ACS Omega 2024, 9, 21851−21863

endogenous antioxidants and classical antioxidants such as vitamin C and selenium.[10] Numerous previous studies have demonstrated the ability of CeO_2 nanozymes alone to treat diseases such as rheumatoid arthritis (RA), inflammatory bowel disease (IBD), and hepatic inflammation, revealing potent anti-inflammatory capabilities and a favorable biosafety profile.[11] However, the therapeutic efficacy of CeO_2 nanozymes for systemic muscle inflammatory degeneration remains undefined.

In this study, we synthesized and characterized CeO_2 nanozymes with an ultrasmall particle size and investigated their catalytic activity and biosafety. Through in vitro experiments, we assessed the potential systemic therapeutic effects of different doses of CeO_2 nanozymes on C2C12 mouse myoblasts by examining their effects on oxidative stress levels and mitochondrial function. Furthermore, we evaluated the efficacy of regular low-dose treatment with CeO_2 nanozymes in adult GDM mouse offspring, specifically focusing on their maximal exercise capacity using a treadmill test. Additionally, we explored the potential mechanism of action of CeO_2 nanozymes in treating systemic inflammatory muscular degeneration through pathology section analysis. Overall, our findings demonstrate the improvement in muscle function in GDM offspring following treatment with CeO_2 nanoenzymes, thereby providing a new reference for the clinical application of these nanoenzymes (Scheme 1).

Scheme 1. CeO_2 Nanoenzymes Improve Skeletal Muscle Function in Gestational Diabetic Offspring[a]

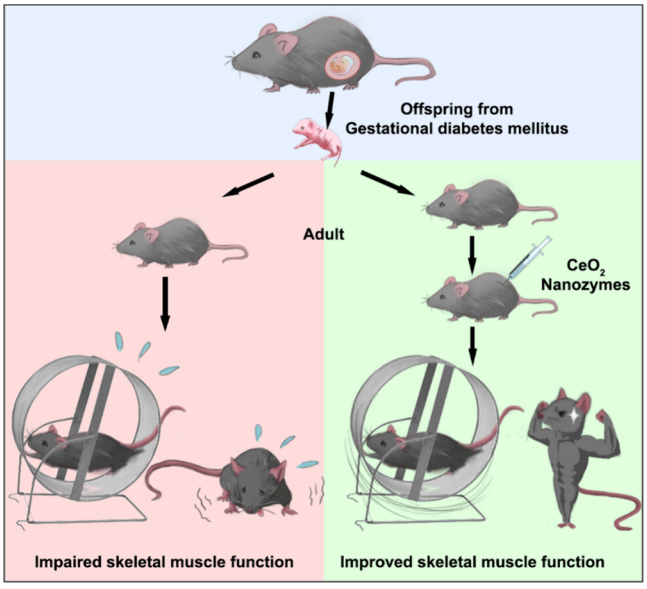

[a]Photograph courtesy of Xinyuan Li. Copyright 2024.

2. MATERIALS AND METHODS

2.1. Synthesis of CNPs. Ce $(NO_3)_3 \cdot 6H_2O$ (1 mmol; Alading, China), Na_3PO_4 (0.01 mmol; Alading, China), PVP (100 mg; Mw 10000, Alading, China), and deionized water (40 mL) were mixed in a hydrothermal synthesis reactor and then maintained at 170 °C for 12 h. The obtained nanoparticle solution was ultracentrifuged at 15,000 g for 10 min and then filtered through a 0.02 μm syringe filter. The final nanoparticle solution was suspended in deionized water or PBS for further studies.

2.2. Characterization. Transmission electron microscopy (TEM; JEM 2100F, Japan) images were used for observing the morphology of the CNPs. The uniform elemental distribution of CNPs was determined using energy-dispersive spectroscopy (EDS; ZEISS GeminiSEM 300) element mapping. Zeta potential analysis was performed using a Malvern ZS-90. XPS was performed using an ESCALAB 250Xi spectrometer. X-ray diffraction (XRD) patterns of CNPs were obtained using an X'Pert PRO MPD X-ray diffractometer.

2.3. Antioxidant Assay. 2,2′-Azinobis(3-ethylbenzthiazoline-6-sulfonate) (ABTS; Alading, China) was used to detect the free radical scavenging ability of ceria nanoparticles. $ABTS^+$ was obtained through incubating 0.8 mL of ABTS (4 mg/mL) with 1 mL of potassium persulfate (1 mg/mL) overnight. 50 μL of $ABTS^+$ was added into 1 mL of CNP solution with different concentration gradients, and the absorption value of $ABTS^+$ at 734 nm was detected. In addition, we used 3,3′,5,5′-tetramethylbenzidine (TMB; Alading, China) with peroxidase to measure antioxidant capacity. The maximum absorbance of •OH can be detected by scanning at 652 nm with a UV−vis spectrophotometer. In addition, the H_2O_2 scavenging activity was used for evaluating the catalytic activity of CNPs, and the H_2O_2 concentration was determined using a hydrogen peroxide assay kit (Solarbio, China).

Intracellular ROS analysis for CNPs was also performed using a DCFH-DA probe (Beyotime, China). In brief, RAW 264.7 macrophage cells were seeded in 96-well plates at a density of 5×10^4 cells/well and cultured overnight. Then, the cell culture media was exchanged with fresh media for the lipopolysaccharide (LPS) group and fresh media with 200 ng/mL LPS for the LPS groups to start stimulation. After 1 h, CNP solutions of different concentrations were added to the cell culture media, and the cells were further incubated for another 24 h. To end LPS stimulation and CeONP treatment, the cells were washed twice with PBS before incubation with a 10 μM DCFH-DA solution for 20 min at 37 °C. At the end of the incubation, the cells were washed and allowed to recover for 5 min at 37 °C. The fluorescence intensity was measured at an excitation wavelength of 492 nm and an emission wavelength of 527 nm.

2.4. In Vitro Biocompatibility Assay. For the in vitro cell viability assay, an MTT [3-(4,5-dimethylthiazol-2-yl)-2,5-diphenyl tetrazolium bromide] assay (Beyotime, China) was performed and used according to the manufacturer's instructions. In brief, after treatment, 20 μL of a 5 mg/mL MTT solution in PBS was added into each well for 4 h. Absorbance was measured by using a microplate reader at 570 nm. The cell viability (%) was evaluated based on the following equation:

$$\text{Cell Viability}(\%) = (\text{ODs} - \text{ODc})/\text{ODc}$$

where ODs and ODc indicate the optical density (OD) value of the sample and control, respectively.

2.5. In Vitro Redox Homeostasis Detect Assay. The JC-1 Staining Kit (Beyotime, Beijing, China) was used to assess mitochondrial membrane potential changes. C2C12 cells were seeded on dishes at a density of 5×10^4 cell/mL and stored overnight. The cells were treated with HG and different concentrations of CNPs for 24 and 48 h. At the end of treatment, cells were removed from the medium, washed three times with PBS, and then incubated with a JC-1 staining kit (20 μM) for 15 min. The JC-1 staining solution was removed, and the cells were washed three times. PBS was added for imaging by CLSM.

https://doi.org/10.1021/acsomega.3c09025
ACS Omega 2024, 9, 21851−21863

The ATP Content Assay Kit (Solarbio, China) was used to assess the ATP levels in CNP-treated C2C12 cells according to the manufacturer's instructions. Luminescence was recorded using a microplate reader.

Mitochondrial stress testing was performed using the Seahorse XF96 extracellular flux analyzer to measure the oxygen consumption rate (OCR) in C2C12 cells. Cells were seeded on a 96-well plate and allowed to adhere overnight. The following day, growth medium was changed 1 h prior to assaying with the Seahorse XF Cell Mito Stress Test Kit. OCR was measured at baseline and following sequential injections of 1 μM oligomycin, 1 μM FCCP, and 0.5 μM rotenone and antimycin A mix. The basal respiration, ATP-linked respiration, proton leak, maximal respiration, reserve capacity, and nonmitochondrial respiration were analyzed.

Detection of mitochondrial complex expression levels was based on WB experiments. Briefly, cultured cells were washed with PBS three times and scraped with cell scrapers, then western lysis buffer was added for 30 min and centrifuged at 12,000 rpm at 4 °C for 15 min, and the supernatant was taken for subsequent experiments. First, the protein concentration was measured with a BCA protein detection kit, then samples with the same amount of protein were added to a 10% SDS polyacrylamide gel for electrophoresis separation, and the proteins on the gel were then transferred to a nitrocellulose filter membrane. The membrane was blocked with 5% bovine serum albumin at room temperature for 1 h, then incubated overnight with primary antibody (1:200, ABclonal, China) at 4 °C, and incubated at room temperature with HRP-conjugated secondary antibody for 1 h. Finally, Western blotting was exposed using an enhanced chemiluminescence kit. In addition, β-actin was used as an internal control.

2.6. In Vitro Anti-inflammatory Assay. After HG-induced C2C12 cells were treated with CNPs, the cells were lysed with an EZ-press RNA purification kit to extract the total RNA. The concentration of the total RNA was measured with a NanoDrop 2000 (Thermo, USA) spectrophotometer and then reverse transcribed RNA into cDNA using a color reverse transcription kit (with gDNA remover). Next, the 2 × Color SYBY Green qPCR master mix and cDNA were mixed well, and the sequence-specific primer pairs (Table S1) of TNF-α, IL1β, IL-6, and GAPDH served as an internal reference. Finally, the fluorescent signal was collected by a real-time PCR system (Applied Biosystems, Thermo Fisher Scientific). For immunofluorescent staining, the C2C12 cells were seeded in a 12-well plate with slices and subjected to the aforementioned method. The treated cells were fixed with 4% paraformaldehyde for 15 min at 4 °C, permeabilized, and blocked with PBS, containing 0.3% Triton X-100, 3% BSA, and goat serum. Thereafter, the cells were stained with a primary antibody (ABclonal, China) at 4 °C overnight. The following day, the cells were incubated with secondary antibodies and DAPI at room temperature for 1 h to avoid lighting. Myotubular crystal violet staining was performed when cells were induced to differentiate by 2% horse serum; 10% crystal violet dye was added and observed. Quantification of myotubes was done by washing them with a 30% acetic acid solution and counting at 550 nm absorbance.

2.7. Animal Experiments. All animal experimental protocols were reviewed and approved by the Fudan University Animal Care and Use Committee (20210325). Eight weeks old C57BL/6J female mice were mated with male mice for 12−18h, and vaginal plugs were checked. Those with sperm plugs were regarded as pregnant for 0.5 days. On day 10.5 of pregnancy, GDM female mice were intraperitoneally injected with streptozotocin (STZ, 150 mg/kg; Sigma, America, S0130), while control mice were injected with the same amount of sodium citrate buffer. Two days after injection, random blood glucose >16.7 mmol/L was considered as a successful model establishment. When 6 weeks old, the GDM offspring mice were intraperitoneally injected with CeO_2−NPs (1.0 mg/kg) twice per week for 4 weeks. At 20 weeks of age, insulin resistance and exercise capacity were examined.

Insulin tolerance test (ITT): Mice were fasted for 4 h, and the baseline blood glucose was measured. Then 0.75 U/kg insulin was injected intraperitoneally, and blood glucose was measured at 30, 60, and 120 min, respectively.

Relative strength of skeletal muscle: The mice were first placed on a stationary platform and allowed to naturally grip the elastic metal strip with all four limbs. Then the elastic metal strip was gradually pulled outward until the mice were unable to maintain their grip, and the strip fell out of their paws. The maximum grip force value was recorded. Relative strength is the maximum grip strength divided by the body weight of the mice.

Maximum exercise capacity: The treadmill was set to run at 6 m/min for 5 min and then increased by 1 m/min at 2 min intervals until the mice were exhausted. The criterion for exhaustion was that the mice remained in the same place after being subjected to more than 6 consecutive shocks within 5 s.

For transcriptomics, quadriceps and tibialis anterior muscles from each group of mice were clipped aseptically and digested into single-cell suspensions. The total cellular RNA was extracted using Trizol (Beyotime; China) and immediately frozen in liquid nitrogen. The libraries were sequenced on a Ilumina Novaseq 6000 platform, and 150 bp paired-end reads were generated. Raw reads of fastq format were first processed using fastp, and the low-quality reads were removed to obtain the clean reads. The clean reads were mapped to the reference genome using HISAT2. FPKM of each gene was calculated, and the read counts of each gene were obtained by HTSeq-count. PCA analyses were performed using *R* (v 3.2.0) to evaluate the biological duplication of samples. Differential expression analysis was performed using the DESeq25. *Q* value <0.05 and foldchange >2 or foldchange <0.5 were set as the thresholds for significantly differential expression genes (DEGs). Hierarchical cluster analysis of DEGs was performed using *R* (v 3.2.0) to demonstrate the expression pattern of genes in different groups and samples. The radar map of top 30 genes was drawn to show the expression of upregulated or downregulated DEGs using *R* packet ggradar. Based on the hypergeometric distribution, GO, KEGG pathway, Reactome, and WikiPathways enrichment analyses of DEGs were performed to screen the significant enriched term using *R* (v 3.2.0), respectively. *R* (v 3.2.0) was used to draw the column diagram, the chord diagram, and the bubble diagram of the significant enrichment term. Gene set enrichment analysis (GSEA) was performed using GSEA software.

2.8. In Vivo Biocompatibility Assay. The biocompatibility of CNPs was monitored using H&E section staining observations of vital organs and blood indices. Intraperitoneal injections were performed on different offspring mice. The major tissues (heart, liver, spleen, lungs, and kidneys) of the offspring mice were dissected for H&E staining at 2 and 6 weeks after intraperitoneal injection, respectively. The blood of offspring mice was collected at the same time point for blood and biochemical examinations. The control group received only

https://doi.org/10.1021/acsomega.3c09025
ACS Omega 2024, 9, 21851−21863

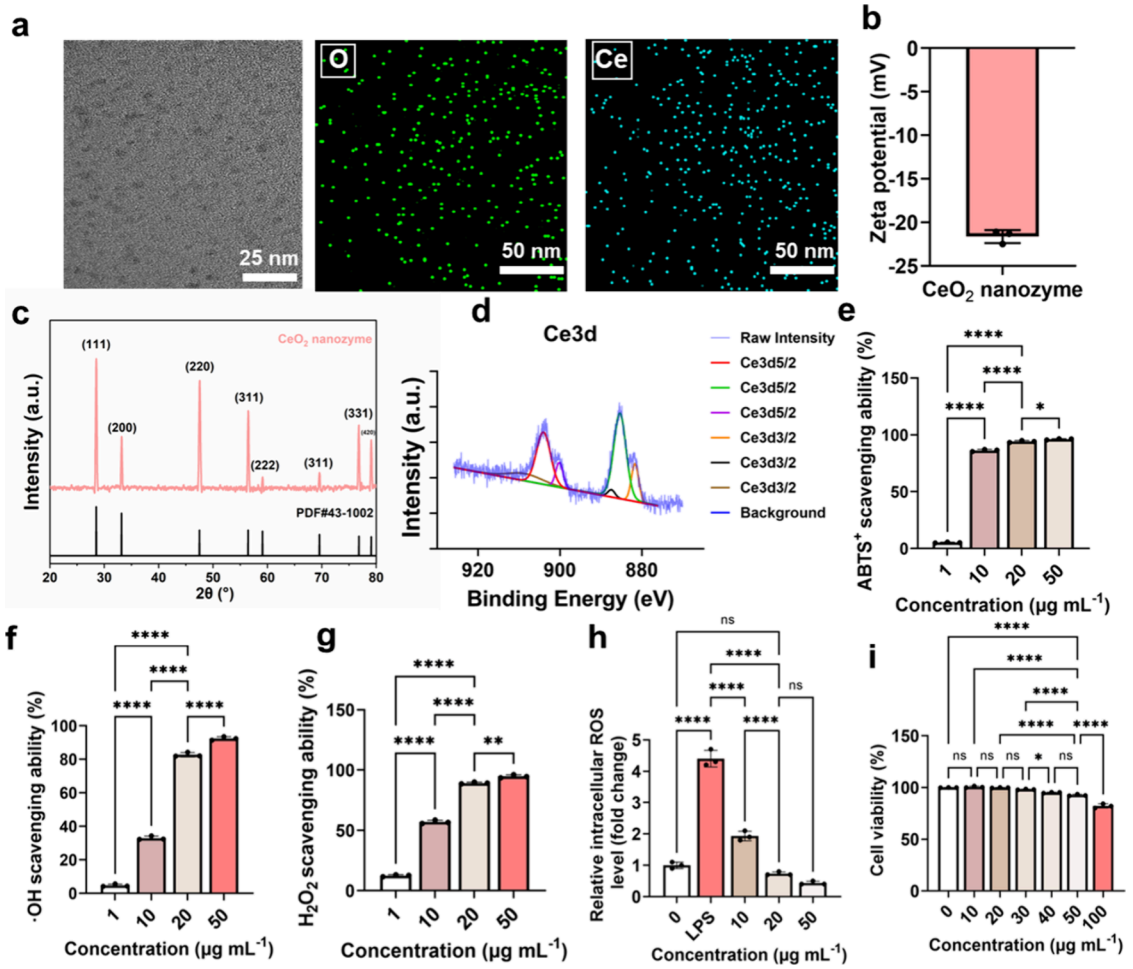

Figure 1. Characteristics of CNPs: (a) TEM and EDS-mapping of CNPs; (b) Zeta potential of CNPs. $n = 3$; (c) XRD spectrum of CNPs and standard XRD PDF; (d) XPS spectrum of Ce 3d of CNPs; (e−g) scavenging test of $ABTS^+$, ·OH, and H_2O_2. $n = 3$; (h) scavenging of intracellular ROS in macrophages by different concentrations of CNPs. $n = 3$; (i) relative cell viability of macrophages treated with different concentrations of CNPs. $n = 3$, $^*p < 0.05$, $^{**}p < 0.01$, $^{***}p < 0.001$, and $^{****}p < 0.0001$, ns means no significant.

PBS treatment and was euthanized at weeks 2 and 6, respectively.

2.9. Statistical Analysis. All data are expressed as the mean ± standard deviation (SD). GraphPad Prism 9 (GraphPad Software Inc., San Diego, CA, USA) was used for statistical analysis. The multiple-comparison tests were performed using one- and two-way analysis of variance (ANOVA). The significant differences between two samples were compared by a two-tailed nonpaired Student's t test. $p < 0.05$ was considered statistically significant.

3. RESULTS AND DISCUSSION

3.1. Characterization and Antioxidant Properties of CNPs. CNPs of ultrasmall size were synthesized through a high-temperature method. Transmission electron microscopy (TEM) images revealed the presence of uniformly sized ultrasmall nanodots with a diameter of approximately 5 nm in the synthesized CNPs (Figures 1a and S1). EDS-mapping indicated a homogeneous distribution of elemental oxygen and cerium, affirming the successful synthesis of the CNPs. Zeta potential analysis suggested a consistently negative charge on the surface of the CNPs, which exhibited an average zeta potential of −21.5 mV, indicating favorable dispersity (Figure 1b). The X-ray diffraction (XRD) pattern showed that the 2θ angles corresponding to the diffraction peaks appearing in the CNP pattern were 28.55°, 33.07°, 47.48°, 56.34°, 59.09°, 69.41°, 76.70°, and 79.08°, respectively, without any spurious peaks observed (Figure 1c). The standard diffraction file (PDF#43−1002) of cerium oxide corresponds to its crystal planes at (110), (200), (220), and (311), respectively. X-ray photoelectron spectroscopy (XPS) was used to evaluate the ratios of Ce (III) and Ce (IV) in the CNPs, revealing that Ce (III) comprised nearly half of the total Ce content, thereby establishing the basis for the excellent antioxidant properties of the CNPs (Figure 1d).

The antioxidant capacity of CNPs was assessed by free radical scavenging experiments conducted at different concentrations.[12] The antioxidant properties of CNPs were detected using probes such as 2,2′-azabis(3-ethylbenzothiazoline 6-sulfonic acid sodium (ABTS) and 3,3′,5,5′-tetramethylbenzidine (TMB). The cation radical $ABTS^+$ exhibited a blue-green color, which reverted to a colorless state in the presence of antioxidants, causing a decrease in the absorption peak at 738 nm. After incubation with CNPs, the characteristic absorption peak of $ABTS^+$ at 738 nm gradually decreased as the concentration of CNPs increased, indicating their strong ability to scavenge ROS (Figure 1e). Similarly, when TMB was incubated with peroxidase, it generated ·OH, which was scavenged by CNPs

https://doi.org/10.1021/acsomega.3c09025
ACS Omega 2024, 9, 21851−21863

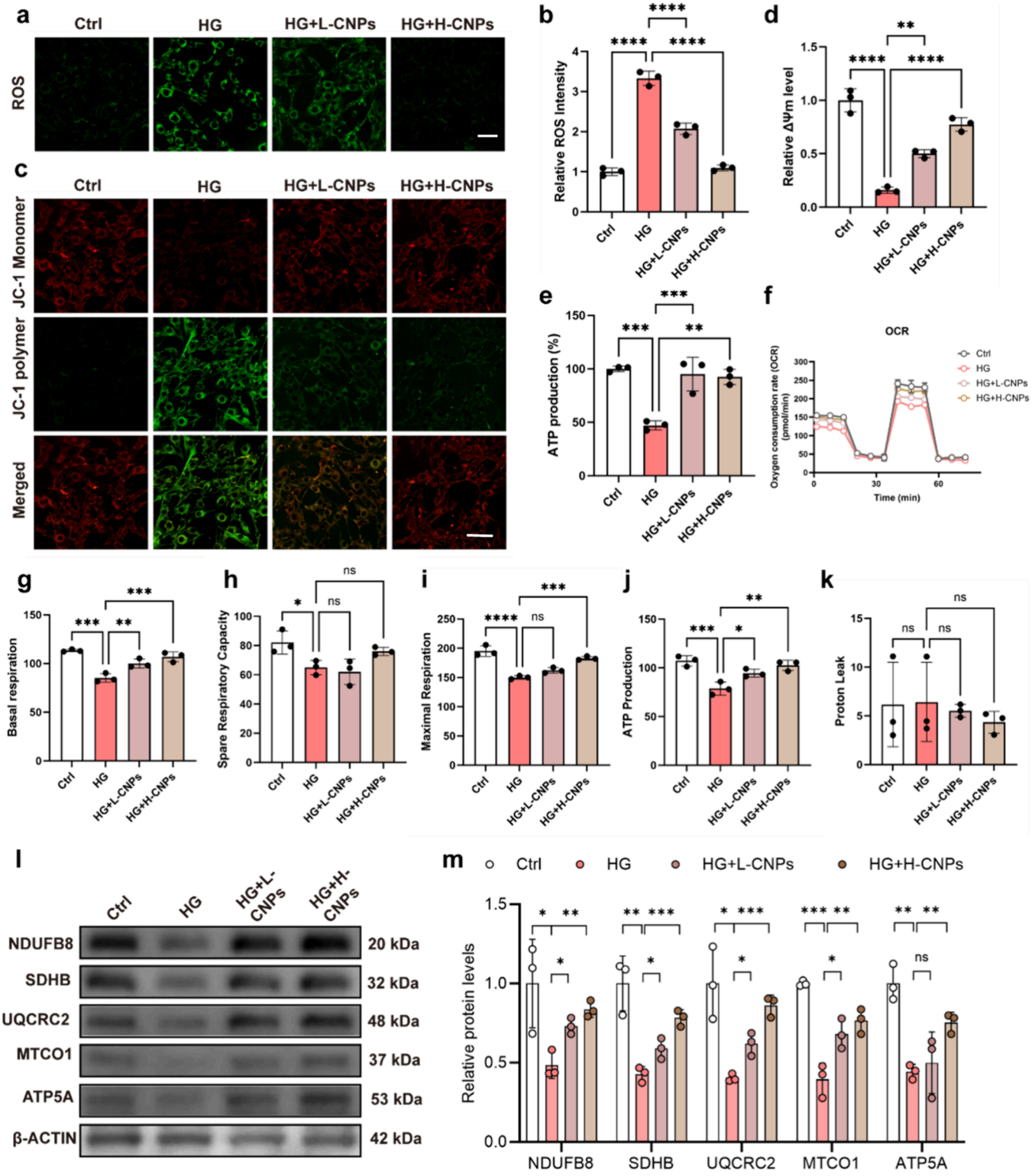

Figure 2. CNPs maintain redox homeostasis in myofibroblasts in vitro: (a, b) Representative intracellular ROS images and corresponding quantification of C2C12 cells after treatment with each group. $n = 3$; (c, d) representative JC-1 staining images and corresponding quantification of C2C12 cells after treatment with each group. $n = 3$; (e) ATP production of C2C12 cells after treatment with each group. $n = 3$; (f–k) representative oxygen consumption rate (OCR) curves and quantification of C2C12 cells after treatment with each group $n = 3$; (l, m) WB test and relative expression of the mitochondrial respiratory chain complex of C2C12 cells after treatment with each group. $n = 3$, $^{*}p < 0.05$, $^{**}p < 0.01$, $^{***}p < 0.001$, and $^{****}p < 0.0001$, ns means no significant. Scale bar = 50 μm.

as the CNP concentration rose (Figure 1f). To assess the hydrogen peroxide scavenging activity, CNPs were mixed with a solution of H_2O_2 (1 M) at different concentrations, and the remaining H_2O_2 content was measured (Figure 1g). The residual H_2O_2 content gradually decreased as the concentration of CNPs increased. Lastly, the intracellular ROS content of the

https://doi.org/10.1021/acsomega.3c09025
ACS Omega 2024, 9, 21851−21863

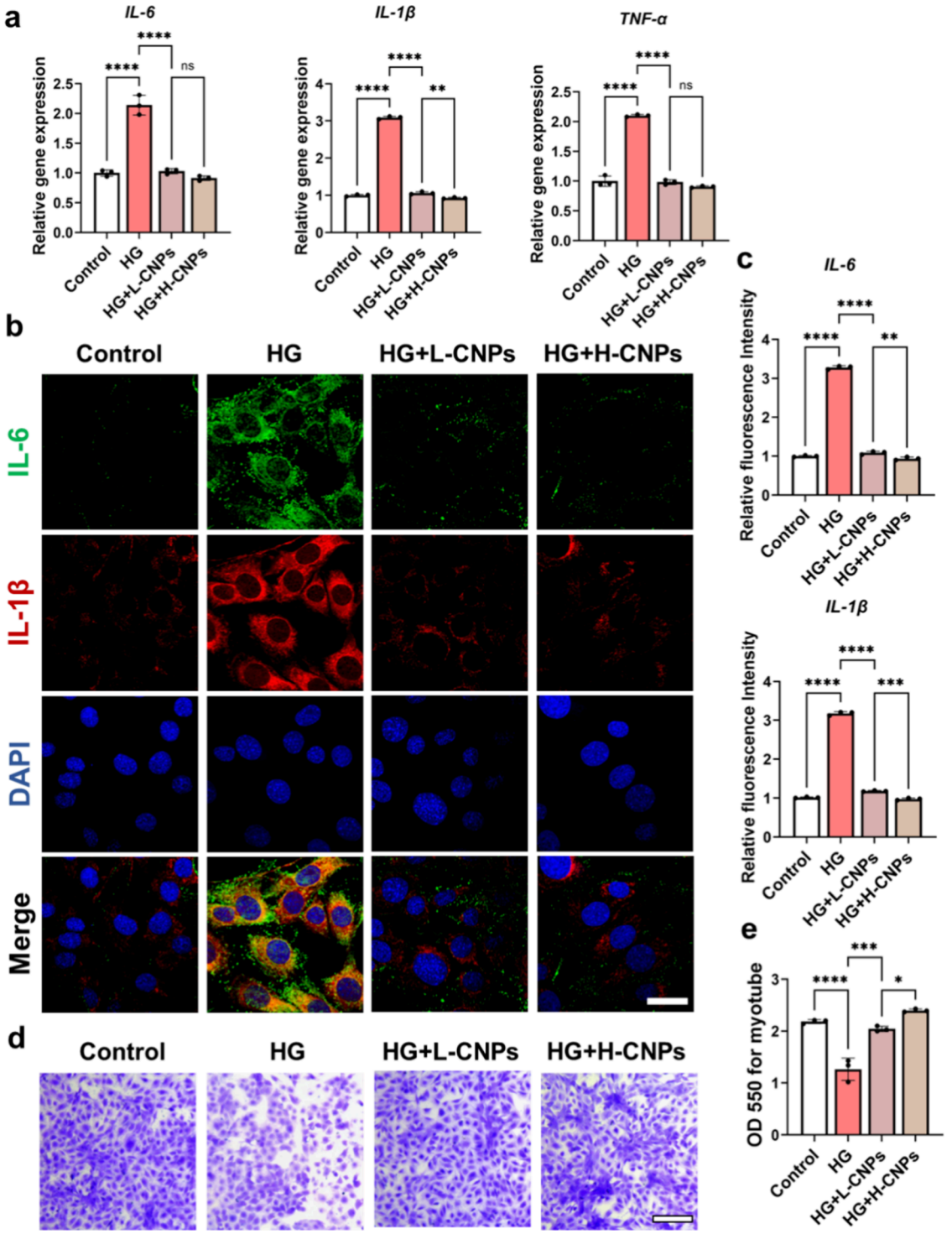

Figure 3. CNPs reduce inflammatory stress in myofibroblasts in vitro: (a) Relative inflammatory gene expression of C2C12 cells after treatment with each group. $n = 3$; (b, c) representative IF images and corresponding quantification of IL-6 and IL-1β of C2C12 cells after treatment with each group. $n = 3$, scale bar = 50 μm.; (d, e) representative crystal violet staining and corresponding quantification of IL-6 and IL-1β of C2C12 cells after treatment with each group. $n = 3$, $^{*}p < 0.05$, $^{**}p < 0.01$, $^{***}p < 0.001$, and $^{****}p < 0.0001$, ns means no significant. Scale bar = 250 μm.

representative immune cell macrophage RAW 264.7 was quantified using DCFH-DA probe incubation and fluorescence zymography after inducing intracellular ROS production with LPS and cocultivation with different concentrations of CNPs.[13,14] As shown in Figure 1h, the intracellular ROS content of macrophages gradually decreased with increasing concentrations of CNPs.

The in vitro biocompatibility of CNPs was evaluated using an MTT assay. The results are shown in Figures 1i and S2. As the concentration of CNPs exceeded 30 μg mL^{-1}, the cell viability of macrophages gradually declined, yet it remained above 90%. Despite the lack of direct reference to therapeutic concentrations in skeletal muscle cells, reference to therapeutic concentrations in previous studies,[15] combined with the results

https://doi.org/10.1021/acsomega.3c09025
ACS Omega 2024, 9, 21851−21863

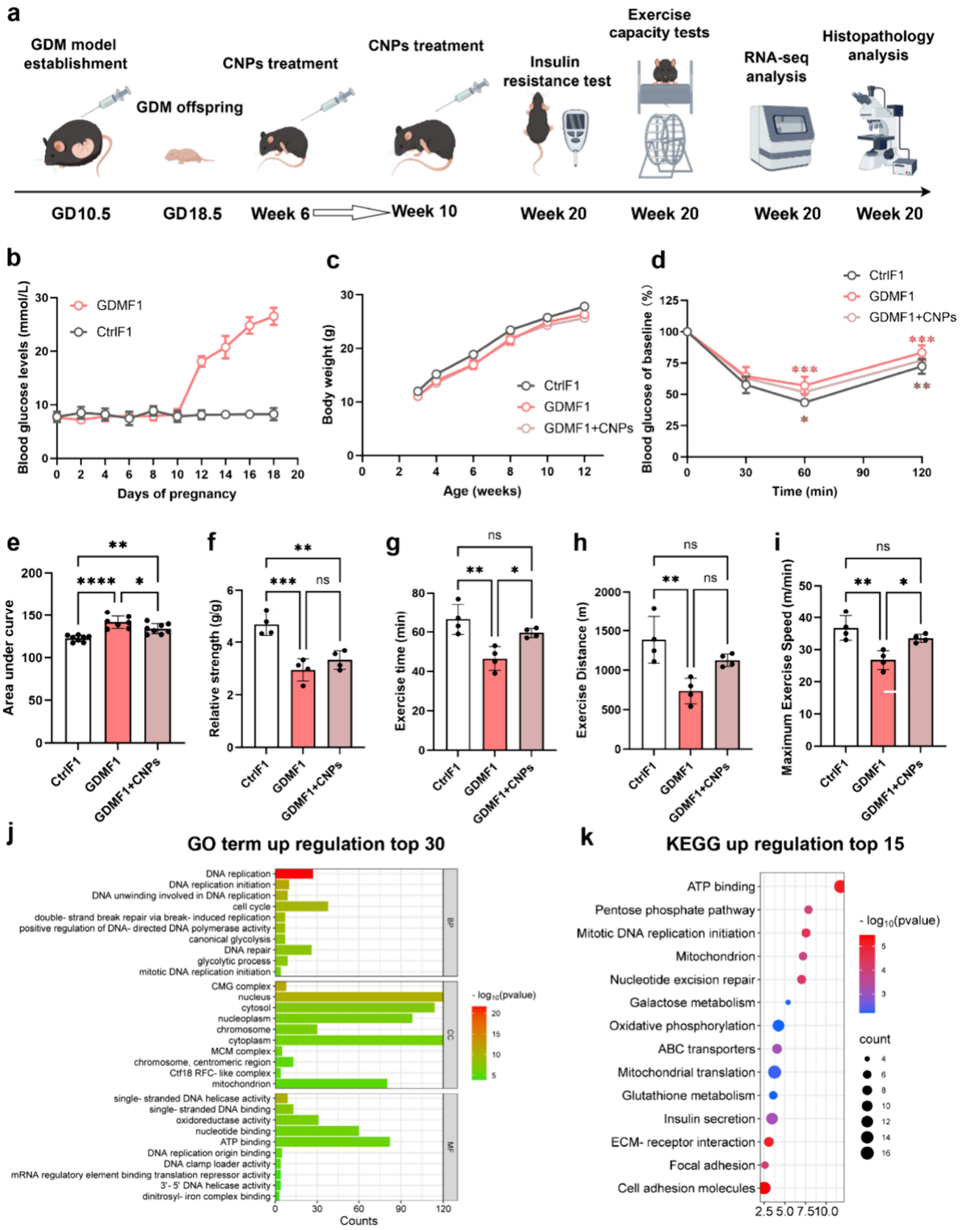

Figure 4. CNPs improve muscle function in GDM offspring in vivo: (a) Flowchart of the intervention protocol for CNPs in GDM offspring; (b) blood glucose levels of the control and GDM group. $n = 5$; (c) body weight of different group offspring. $n = 5$; (d, e) ITT and corresponding quantification of different group offspring. $n = 8$; (f) relative strength of different group offspring. $n = 4$; (g–i) maximal exercise capacity of different group offspring. $n = 4$; (j) top 30 upregulated pathways differentially enriched for GO Term after CNP treatment compared to GDM offspring. (k) Top 15 upregulated pathways differentially enriched for KEGG after CNP treatment compared to GDM offspring. *$p < 0.05$, **$p < 0.01$, ***$p < 0.001$, and ****$p < 0.0001$, ns means no significant. Photograph courtesy of Wanbo Zhu. Copyright 2024.

https://doi.org/10.1021/acsomega.3c09025
ACS Omega 2024, 9, 21851−21863

of the in vitro antioxidant experiments, we chose 20 and 50 μg mL^{-1} as the low-dose and high-dose CNPs, respectively, for further examination of muscle function and mitochondrial homeostasis in GDM offspring.

3.2. CNPs Maintain Redox Homeostasis in Myofibroblasts In Vitro. To replicate the functional inflammatory degeneration of muscle in GDM offspring in vitro, we cultured mouse myoblasts C2C12 in a high glucose medium (HG) to mimic GDM offspring. We then added low-dose CNPs (L-CNPs) and high-dose CNPs (H−CNPs) as the treatment groups.[16] The intracellular ROS content in C2C12 was measured, and confocal laser scanning microscopy (CLSM) was used to observe the antioxidant effect of CNPs on C2C12 cells in high glucose medium (Figure 2a,b). Mitochondrial membrane potential staining was used to assess the ability of CNPs to regulate mitochondrial function in high-glucose-medium-induced C2C12 cells. As shown in Figure 2c, the mitochondrial membrane potential of C2C12 decreased in the HG group, and the intensity of green fluorescence, which represents the JC-1 polymer, decreased upon the addition of CNPs, indicating the role of CNPs in the maintenance of mitochondrial homeostasis (Figure 2d). Moreover, we confirmed that CNPs promote mitochondrial function in myoblasts through an ATP generation assay, as CNPs significantly reversed the low ATP generation in high glucose medium (Figure 2e).

Aerobic respiration of cells can be measured by the rate at which cells consume extracellular oxygen concentration.[17] To further evaluate the maintenance of mitochondrial homeostasis in adult myocytes by CNPs, the aerobic respiration of cells was assessed using the OCR, which reflects the function of cellular mitochondria.[18] Figure 2f,g demonstrates that the HG group showed impaired basal respiration of C2C12 cells, while the intervention of CNPs improved the basal respiration rate. Additionally, the maximal respiration of C2C12 cells induced by FCCP was significantly reduced in the HG group, but this downward trend was reversed by the intervention of CNPs, indicating that CNPs maintain cellular mitochondrial homeostasis by regulating the oxidative phosphorylation of C2C12 cells (Figure 2h). Treatment with CNPs also rescued spare respiratory capacity, ATP production, and proton leak of C2C12 cells in the HG group (Figure 2i−k). The expression of mitochondrial respiratory chain complex I (NDUFB8), complex II (SDHB), complex III (Uqcrc2), complex IV (MTCO1), and complex V (ATP5A) in C2C12 cells showed significant restrictions in mitochondrial function under high glucose conditions (Figure 2l,m).[19]

3.3. CNPs Reduce Inflammatory Stress in Myofibroblasts In Vitro. The scavenging of intracellular ROS by CNPs, along with their ability to restore mitochondrial function and maintain cellular redox homeostasis, contributes to the reduction of inflammatory stress and the restoration of cellular function in myofibroblasts.[14,20] The expression of inflammation-related genes in myofibroblasts was initially detected using qPCR, and the results are shown in Figure 3a. In the HG group, IL-1β, IL-6, and TNF-α genes in C2C12 cells were significantly overexpressed in the HG group. However, the addition of CNPs resulted in a significant downregulation of proinflammatory gene expression, suggesting a potential anti-inflammatory effect. IF staining and CLSM were used to observe the expression of IL-6 in C2C12 following different interventions, and the results are shown in Figure 3b,c. The addition of CNPs significantly downregulated the expression of IL-6 in the HG group, validating the results of qPCR and confirming the down-regulation of the inflammatory contingency of C2C12 cells by CNPs.

Myotubular function is the predominant cellular behavior of myofibroblasts to maintain normal muscle homeostasis. C2C12 cell function was evaluated by myotube formation induction and crystal violet staining (Figure 3d,e). The results indicated that the myotube content represented by a high concentration of crystal violet was significantly reduced in the HG group, while the intervention of CNPs promoted myotube formation in C2C12 cells.[21] Combined with the regulation of IL-1β by CNPs and based on the previous findings, the reason for this discrepancy may be that CNPs inhibit the expression and release of IL-1β, which further inhibits the activation of the NLRP3 inflammasome and the downstream inflammatory disturbances within the myocytes, thus maintaining myocyte homeostasis.[22]

3.4. CNPs Improve Muscle Function in GDM Offspring In Vivo. The CNPs intervention protocol in GDM offspring is shown in the flowchart (Figure 4a). CNPs were administered to the GDM offspring from weeks 6 to 10. Continuous testing of blood glucose showed that blood glucose levels spiked in the GDM group on gestational day 12.5 and remained at high levels until delivery, which indicated successful modeling of GDM (Figure 4b).[3,23] Body weight monitoring of the offspring in each group showed that both the GDM offspring and the GDM +CNPs offspring had slightly smaller body weights compared to those in the control group (Figure 4c). Additionally, the results of the ITT demonstrated that the GDM offspring had significantly higher insulin resistance than the control offspring, and the intake of CNPs improved insulin resistance in the GDM offspring, suggesting a potential therapeutic effect of CNPs (Figure 4d,e). Skeletal muscle function and exercise capacity were assessed in GDM offspring at week 20. First, the muscle function of the offspring in each group was assessed using the mouse maximal muscle strength test. The administration of CNPs partially improved the relative muscle strength of the GDM offspring (Figure 4f). Furthermore, the maximal exercise capacity of the offspring mice in each group was evaluated using the treadmill exercise test. The administration of CNPs partially improved the maximal exercise distance and significantly enhanced the maximal exercise time and speed of the GDM offspring, approaching that of the control offspring (Figure 4g−i). These experiments confirmed that the intake of CNPs could improve the muscle function and locomotor capacity of the GDM offspring.

To further investigate the potential mechanism of systemic treatment of GDM offspring with CNPs, gastrocnemius and tibialis anterior muscles from mice treated with CNPs and GDM mice were collected for RNA-seq. GO Term and KEGG enrichment analyses suggested that signaling pathways related to ATP binding, oxidative phosphorylation, mitochondrial membrane stability, and DNA replication were upregulated in mice treated with CNPs (Figure 4j,k). This is similar to previous studies of systemic treatment with CNPs, suggesting the rescue of mitochondrial function and maintenance of mitochondrial homeostasis by CNPs.

3.5. CNPs Treat GDM Offspring by Attenuating Mitochondrial Oxidative Stress In Vivo. Further GSEA analysis of the RNA-seq transcriptome results revealed that the CNPs-treated group was significantly more enriched in the mitochondrial-oxidative-stress-related signaling pathway than in the other pathways. Differential gene expression of oxidative phosphorylation pathways in muscles treated with CNPs is

https://doi.org/10.1021/acsomega.3c09025
ACS Omega 2024, 9, 21851−21863

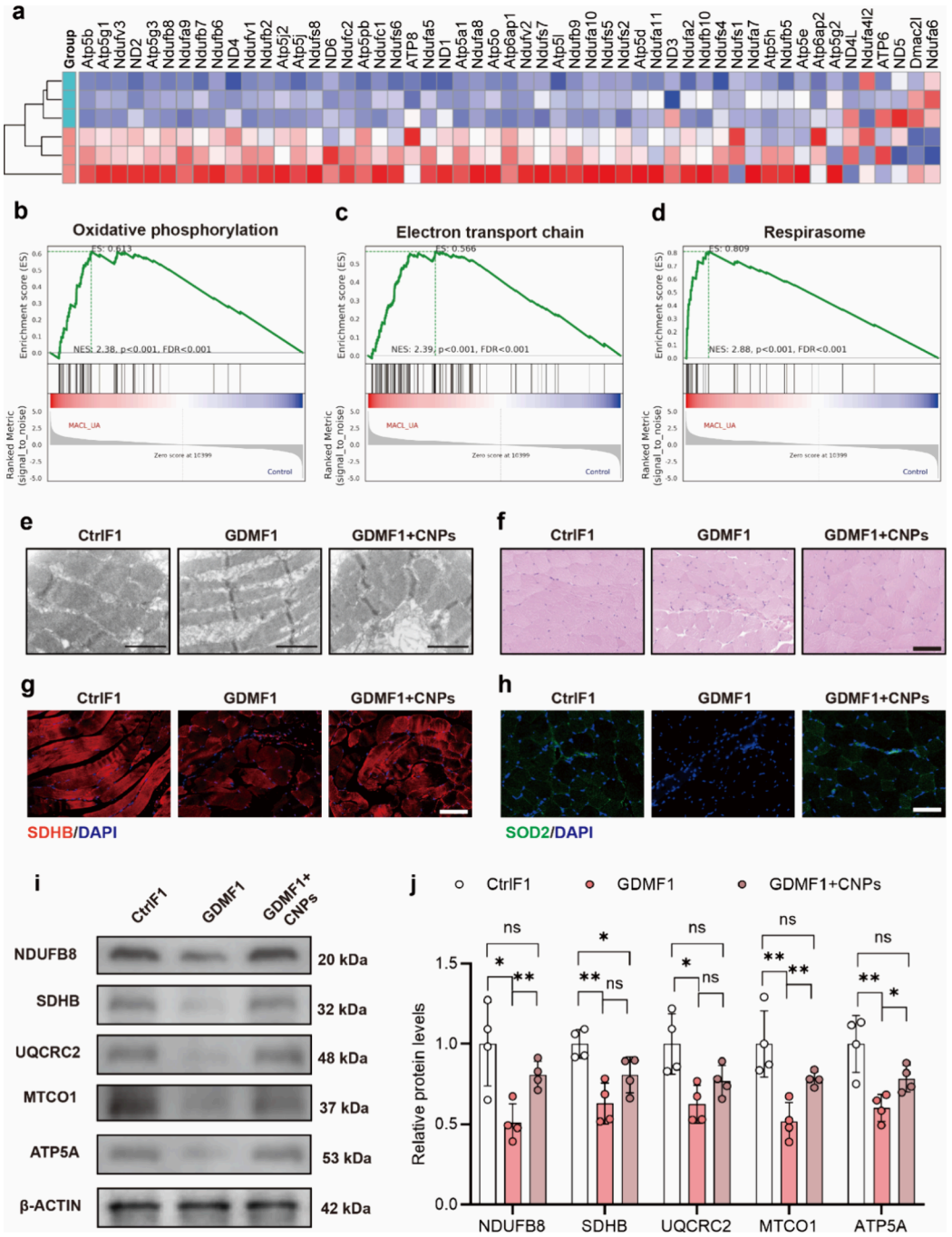

Figure 5. CNPs treat GDM offspring by attenuating mitochondrial oxidative stress in vivo: (a) Heatmap of differentially expressed genes in the oxidative phosphorylation signaling pathway after treatment of CNPs compared to controls; (b−d) representative results of GSEA analysis after treatment of CNPs compared to controls; (e) representative TEM image of the quadriceps of different group offspring. n = 4, scale bar = 50 μm; (f) H&E staining of muscle tissue sections after treatment in each group, scale bar = 50 μm. (g, h) Immunofluorescence-stained sections of muscle tissue after treatment in each group. SDHB in red, SOD2 in green, and DAPI in blue; scale bar = 50 μm. (i, j) WB test and relative expression of the mitochondrial respiratory chain complex of different group offspring. n = 4, *p < 0.05, **p < 0.01, ***p < 0.001, and ****p < 0.0001, ns means no significant.

demonstrated in Figure 5a, showing differential expression of major genes related to oxidative phosphorylation metabolism. GSEA analysis including oxidative phosphorylation, electron transport chain, and respirasome showed significantly up-regulated differential expression, suggesting that CNPs achieve regulation of mitochondrial homeostasis by attenuating mitochondrial oxidative stress (Figure 5b−d).

To validate the potential mechanisms of CNPs suggested in transcriptomics, the muscle sections of quadriceps muscle from each group of offspring were observed using TEM, as shown in Figure 5e. Muscle sections based on hematoxylin-eosin (H&E) staining suggested slight disorganization of muscle texture in GDM offspring, whereas both GDM offspring treated with CNPs and control offspring showed regular cross-sectional muscle texture structure. In addition, a small amount of

https://doi.org/10.1021/acsomega.3c09025
ACS Omega 2024, 9, 21851−21863

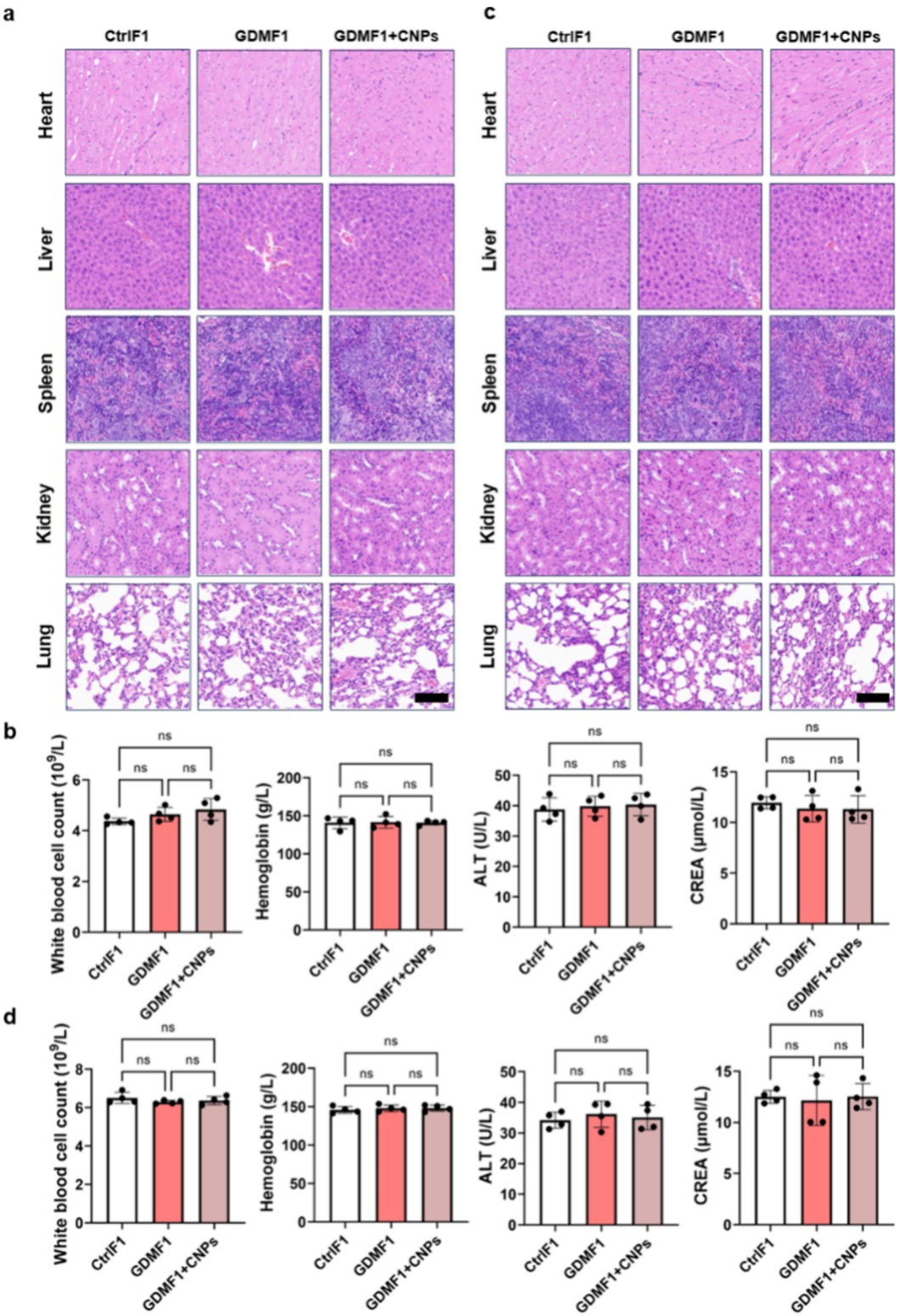

Figure 6. Biocompatibility of CNPs in vivo: (a, b) H&E-stained sections of vital organs (heart, liver, spleen, lungs, and kidneys) as well as peripheral blood test results (white blood cell count, hemoglobin, alanine aminotransferase (ALT), and blood creatinine (CREA) test results of different group offspring at week 12. $n = 5$. Scale bar = 250 μm; (c, d) H&E-stained sections of vital organs and peripheral blood test results of different group offspring at week 16. $n = 5$, $^{*}p < 0.05$, $^{**}p < 0.01$, $^{***}p < 0.001$, and $^{****}p < 0.0001$, ns means no significant.

inflammatory cell infiltration was observed in GDM offspring treated with the CNPs group compared to GDM offspring not receiving CNP treatment group (Figures 5f and S3). The administration of CNPs improved the mitochondrial morphology and increased the number of mitochondria in the GDM offspring. Immunofluorescence of SDHB and SOD2 revealed that CNPs could alleviate SDH expression impairment in the skeletal muscle of offspring caused by GDM (Figures 5g,h and S4). The enhancement of mitochondrial respiratory chain complex I (NDUFB8), complex II (SDHB), complex III

https://doi.org/10.1021/acsomega.3c09025
ACS Omega 2024, 9, 21851−21863

(Uqcrc2), complex IV (MTCO1), and complex V (ATP5A) expression as a result of CNP uptake was verified through total protein extraction and a WB test on muscle tissue homogenates (Figure 5i,j). Overall, the in vivo experiments confirmed that CNPs improve skeletal muscle function and exercise capacity in GDM offspring by modulating mitochondrial homeostasis and respiratory chain function.

3.6. Biocompatibility of CNPs In Vivo. The biocompatibility assessment of GDM offspring treated with CNPs was performed at weeks 12 and 16, respectively.[24] Figure 6a displays the H&E-stained sections of vital organs such as the heart, liver, spleen, lungs, and kidneys. Additionally, peripheral blood test results, including white blood cell count, hemoglobin, alanine aminotransferase (ALT), and blood creatinine (CREA) test results of the CNPs-treated GDM offspring mice at week 12, were compared to those of the control group (Figure 6b). No significant differences were observed. Similarly, the observation of H&E-stained sections of vital organs and peripheral blood test results at week 16 did not show any significant differences between the CNPs-treated GDM offspring and the control group, indicating a favorable mid- to long-term biosafety following CNP treatment (Figure 6c,d).

4. CONCLUSIONS

In summary, we synthesized ultrasmall particle size CNPs for improving muscle function and locomotor capacity in GDM offspring. In vitro experiments revealed that CNPs can effectively eliminate excess ROS from muscle cells, restore mitochondrial homeostasis, and improve the respiratory chain complex function. Furthermore, CNPs exhibited anti-inflammatory properties and restored normal muscle cell myotube-forming capacity. In in vivo experiments, GDM offspring treated with CNPs from weeks 6 to 10 showed significant improvements in muscle strength and maximal exercise capacity. TEM sections of muscle tissues and protein expression analysis confirmed the regulation of mitochondrial function by CNPs. Importantly, mid- and long-term biocompatibility assessments verified the biosafety of CNPs. Therefore, CNPs offer a new approach for treating GDM offspring and provide hope for nonpharmacological improvement of muscle function.

■ ASSOCIATED CONTENT

Supporting Information

The Supporting Information is available free of charge at https://pubs.acs.org/doi/10.1021/acsomega.3c09025.

Nanoparticle size distribution; CCK-8 analysis; immunofluorescence-stained sections and fluorescence intensity of muscle tissue; and primer sequences used in this experiment (PDF)

■ AUTHOR INFORMATION

Corresponding Authors

Guolian Ding − *Obstetrics and Gynecology Hospital, Institute of Reproduction and Development, Fudan University, Shanghai 200433, China; Research Units of Embryo Original Diseases, Chinese Academy of Medical Sciences (No. 2019RU056), Shanghai 200011, China*; Email: dingguolian@fudan.edu.cn

Hefeng Huang − *Obstetrics and Gynecology Hospital, Institute of Reproduction and Development, Fudan University, Shanghai 200433, China; Research Units of Embryo Original Diseases, Chinese Academy of Medical Sciences (No. 2019RU056), Shanghai 200011, China; Key Laboratory of Reproductive Genetics (Ministry of Education), Department of Reproductive Endocrinology, Women's Hospital, Zhejiang University School of Medicine, Hangzhou 310058, China*; Email: huanghefg@fudan.edu.cn

Authors

Xinyuan Li − *Obstetrics and Gynecology Hospital, Institute of Reproduction and Development, Fudan University, Shanghai 200433, China; Research Units of Embryo Original Diseases, Chinese Academy of Medical Sciences (No. 2019RU056), Shanghai 200011, China; Key Laboratory of Reproductive Genetics (Ministry of Education), Department of Reproductive Endocrinology, Women's Hospital, Zhejiang University School of Medicine, Hangzhou 310058, China*

Wanbo Zhu − *Department of Orthopedics, Shanghai Sixth People's Hospital Affiliated to Shanghai Jiao Tong University School of Medicine, Shanghai Jiao Tong University, Shanghai 200233, China*; orcid.org/0000-0003-3457-3432

Rui Liu − *Obstetrics and Gynecology Hospital, Institute of Reproduction and Development, Fudan University, Shanghai 200433, China; Research Units of Embryo Original Diseases, Chinese Academy of Medical Sciences (No. 2019RU056), Shanghai 200011, China; Key Laboratory of Reproductive Genetics (Ministry of Education), Department of Reproductive Endocrinology, Women's Hospital, Zhejiang University School of Medicine, Hangzhou 310058, China; Reproductive Medicine Center, International Institutes of Medicine, the Fourth Affiliated Hospital, Zhejiang University School of Medicine, Yiwu 322000, China*

Complete contact information is available at: https://pubs.acs.org/10.1021/acsomega.3c09025

Author Contributions

X.L. and W.Z. contributed equally to this work. All authors approved the final version of this manuscript.

Notes

The authors declare no competing financial interest.

■ ACKNOWLEDGMENTS

This work is supported by the National Key R&D Program of China (2022YFC2703500), the National Natural Science Foundation of China (82088102), the CAMS Innovation Fund for Medical Sciences (2019-I2M-5-064), the Collaborative Innovation Program of Shanghai Municipal Health Commission (2020CXJQ01), the Clinical Research Plan of SHDC (SHDC2020CR1008A), the Shanghai Clinical Research Center for Gynecological Diseases (22MC1940200), the Shanghai Urogenital System Diseases Research Center (2022ZZ01012), and the Shanghai Frontiers Science Research Center of Reproduction and Development.

■ REFERENCES

(1) Zhu, H.; Chen, B.; Cheng, Y.; Zhou, Y.; Yan, Y. S.; Luo, Q.; Jiang, Y.; Sheng, J. Z.; Ding, G. L.; Huang, H. F. Insulin Therapy for Gestational Diabetes Mellitus Does Not Fully Protect Offspring From Diet-Induced Metabolic Disorders. *Diabetes* **2019**, *68* (4), 696−708.

(2) Nicholas, L. M.; Morrison, J. L.; Rattanatray, L.; Zhang, S.; Ozanne, S. E.; McMillen, I. C. The early origins of obesity and insulin resistance: timing, programming and mechanisms. *Int. J. Obes (Lond)* **2016**, *40* (2), 229−238. Holemans, K.; Gerber, R. T.; Meurrens, K.; De Clerck, F.; Poston, L.; Van Assche, F. A. Streptozotocin diabetes in the pregnant rat induces cardiovascular dysfunction in adult offspring.

Diabetologia **1999**, *42* (1), 81−89. Zou, K.; Ren, J.; Luo, S.; Zhang, J.; Zhou, C.; Tan, C.; Lv, P.; Sun, X.; Sheng, J.; Liu, X.; et al. Intrauterine hyperglycemia impairs memory across two generations. *Transl Psychiatry* **2021**, *11* (1), 434.

(3) Ding, G. L.; Wang, F. F.; Shu, J.; Tian, S.; Jiang, Y.; Zhang, D.; Wang, N.; Luo, Q.; Zhang, Y.; Jin, F.; et al. Transgenerational glucose intolerance with Igf2/H19 epigenetic alterations in mouse islet induced by intrauterine hyperglycemia. *Diabetes* **2012**, *61* (5), 1133−1142.

(4) Morino, K.; Petersen, K. F.; Dufour, S.; Befroy, D.; Frattini, J.; Shatzkes, N.; Neschen, S.; White, M. F.; Bilz, S.; Sono, S.; et al. Reduced mitochondrial density and increased IRS-1 serine phosphorylation in muscle of insulin-resistant offspring of type 2 diabetic parents. *J. Clin Invest* **2005**, *115* (12), 3587−3593. Latouche, C.; Heywood, S. E.; Henry, S. L.; Ziemann, M.; Lazarus, R.; El-Osta, A.; Armitage, J. A.; Kingwell, B. A. Maternal overnutrition programs changes in the expression of skeletal muscle genes that are associated with insulin resistance and defects of oxidative phosphorylation in adult male rat offspring. *J. Nutr.* **2014**, *144* (3), 237−244. Kua, K. L.; Hu, S.; Wang, C.; Yao, J.; Dang, D.; Sawatzke, A. B.; Segar, J. L.; Wang, K.; Norris, A. W. Fetal hyperglycemia acutely induces persistent insulin resistance in skeletal muscle. *J. Endocrinol* **2019**, *242* (1), M1−M15.

(5) McMurray, F.; MacFarlane, M.; Kim, K.; Patten, D. A.; Wei-LaPierre, L.; Fullerton, M. D.; Harper, M. E. Maternal diet-induced obesity alters muscle mitochondrial function in offspring without changing insulin sensitivity. *FASEB J.* **2019**, *33* (12), 13515−13526. Fujimaki, S.; Kuwabara, T. Diabetes-Induced Dysfunction of Mitochondria and Stem Cells in Skeletal Muscle and the Nervous System. *Int. J. Mol. Sci.* **2017**, *18* (10), 2147.

(6) Singh, N.; Sherin, G. R.; Mugesh, G. Antioxidant and Prooxidant Nanozymes: From Cellular Redox Regulation to Next-Generation Therapeutics. *Angew. Chem., Int. Ed. Engl.* **2023**, *62* (33), No. e202301232. Xu, D. T.; Wu, L. Y.; Yao, H. D.; Zhao, L. N. Catalase-Like Nanozymes: Classification, Catalytic Mechanisms, and Their Applications. *Small* **2022**, *18* (37), No. 2203400. Zhao, H.; Zhang, R.; Yan, X.; Fan, K. Superoxide dismutase nanozymes: an emerging star for anti-oxidation. *J. Mater. Chem. B* **2021**, *9* (35), 6939−6957.

(7) Ghorbani, M.; Izadi, Z.; Jafari, S.; Casals, E.; Rezaei, F.; Aliabadi, A.; Moore, A.; Ansari, A.; Puntes, V.; Jaymand, M.; et al. Preclinical studies conducted on nanozyme antioxidants: shortcomings and challenges based on US FDA regulations. *Nanomedicine (Lond)* **2021**, *16* (13), 1133−1151. Li, H.; Xia, P.; Pan, S.; Qi, Z.; Fu, C.; Yu, Z.; Kong, W.; Chang, Y.; Wang, K.; Wu, D.; et al. The Advances of Ceria Nanoparticles for Biomedical Applications in Orthopaedics. *Int. J. Nanomedicine* **2020**, *15*, 7199−7214.

(8) Feng, N.; Liu, Y.; Dai, X.; Wang, Y.; Guo, Q.; Li, Q. Advanced applications of cerium oxide based nanozymes in cancer. *RSC Adv.* **2022**, *12* (3), 1486−1493.

(9) Singh, S. Cerium oxide based nanozymes: Redox phenomenon at biointerfaces. *Biointerphases* **2016**, *11* (4), No. 04b202. Baldim, V.; Yadav, N.; Bia, N.; Graillot, A.; Loubat, C.; Singh, S.; Karakoti, A. S.; Berret, J. F. Polymer-Coated Cerium Oxide Nanoparticles as Oxidoreductase-like Catalysts. *Acs Appl. Mater. Inter* **2020**, *12* (37), 42056−42066.

(10) Saifi, M. A.; Seal, S.; Godugu, C. Nanoceria, the versatile nanoparticles: Promising biomedical applications. *J. Controlled Release* **2021**, *338*, 164−189.

(11) Wu, Y.; Yang, Y. C.; Zhao, W.; Xu, Z. P.; Little, P. J.; Whittaker, A. K.; Zhang, R.; Ta, H. T. Novel iron oxide-cerium oxide core-shell nanoparticles as a potential theranostic material for ROS related inflammatory diseases. *J. Mater. Chem. B* **2018**, *6* (30), 4937−4951. Kalashnikova, I.; Chung, S. J.; Nafiujjaman, M.; Hill, M. L.; Siziba, M. E.; Contag, C. H.; Kim, T. Ceria-based nanotheranostic agent for rheumatoid arthritis. *Theranostics* **2020**, *10* (26), 11863−11880. Naha, P. C.; Hsu, J. C.; Kim, J.; Shah, S.; Bouche, M.; Si-Mohamed, S.; Rosario-Berrios, D. N.; Douek, P.; Hajfathalian, M.; Yasini, P.; et al. Dextran-Coated Cerium Oxide Nanoparticles: A Computed Tomography Contrast Agent for Imaging the Gastrointestinal Tract and Inflammatory Bowel Disease. *ACS Nano* **2020**, *14* (8), 10187−10197. Cao, Y.; Cheng, K.; Yang, M.; Deng, Z.; Ma, Y.; Yan, X.; Zhang, Y.; Jia, Z.; Wang, J.; Tu, K.; et al. Orally administration of cerium oxide nanozyme for computed tomography imaging and anti-inflammatory/anti-fibrotic therapy of inflammatory bowel disease. *J. Nanobiotechnology* **2023**, *21* (1), 21. Oro, D.; Yudina, T.; Fernandez-Varo, G.; Casals, E.; Reichenbach, V.; Casals, G.; Gonzalez de la Presa, B.; Sandalinas, S.; Carvajal, S.; Puntes, V.; et al. Cerium oxide nanoparticles reduce steatosis, portal hypertension and display anti-inflammatory properties in rats with liver fibrosis. *J. Hepatol* **2016**, *64* (3), 691−698. Zhang, S.; Cao, Y.; Xu, B.; Zhang, H.; Zhang, S.; Sun, J.; Tang, Y.; Wang, Y. An antioxidant nanodrug protects against hepatic ischemia-reperfusion injury by attenuating oxidative stress and inflammation. *J. Mater. Chem. B* **2022**, *10* (37), 7563−7569.

(12) Li, X.; Han, Z.; Wang, T.; Ma, C.; Li, H.; Lei, H.; Yang, Y.; Wang, Y.; Pei, Z.; Liu, Z.; et al. Cerium oxide nanoparticles with antioxidative neurorestoration for ischemic stroke. *Biomaterials* **2022**, *291*, No. 121904. Augustine, R.; Zahid, A. A.; Hasan, A.; Dalvi, Y. B.; Jacob, J. Cerium Oxide Nanoparticle-Loaded Gelatin Methacryloyl Hydrogel Wound-Healing Patch with Free Radical Scavenging Activity. *ACS Biomater Sci. Eng.* **2021**, *7* (1), 279−290.

(13) Wu, Y.; Ta, H. T. Different approaches to synthesising cerium oxide nanoparticles and their corresponding physical characteristics, and ROS scavenging and anti-inflammatory capabilities. *J. Mater. Chem. B* **2021**, *9* (36), 7291−7301.

(14) Wei, F.; Neal, C. J.; Sakthivel, T. S.; Kean, T.; Seal, S.; Coathup, M. J. Multi-functional cerium oxide nanoparticles regulate inflammation and enhance osteogenesis. *Mater. Sci. Eng. C Mater. Biol. Appl.* **2021**, *124*, No. 112041.

(15) Datta, A.; Mishra, S.; Manna, K.; Das Saha, K.; Mukherjee, S.; Roy, S. Pro-Oxidant Therapeutic Activities of Cerium Oxide Nanoparticles in Colorectal Carcinoma Cells. *ACS Omega* **2020**, *5* (17), 9714−9723. Pagliari, F.; Mandoli, C.; Forte, G.; Magnani, E.; Pagliari, S.; Nardone, G.; Licoccia, S.; Minieri, M.; Di Nardo, P.; Traversa, E. Cerium Oxide Nanoparticles Protect Cardiac Progenitor Cells from Oxidative Stress. *ACS Nano* **2012**, *6* (5), 3767−3775.

(16) Yano, N.; Zhang, L.; Wei, D.; Dubielecka, P. M.; Wei, L.; Zhuang, S.; Zhu, P.; Qin, G.; Liu, P. Y.; Chin, Y. E.; et al. Irisin counteracts high glucose and fatty acid-induced cytotoxicity by preserving the AMPK-insulin receptor signaling axis in C2C12 myoblasts. *Am. J. Physiol Endocrinol Metab* **2020**, *318* (5), E791−E805. Andrews-Guzman, M.; Ruz, M.; Arredondo-Olguin, M. Zinc Modulates the Response to Apoptosis in an In Vitro Model with High Glucose and Inflammatory Stimuli in C2C12 Cells. *Biol. Trace Elem Res.* **2021**, *199* (6), 2288−2294.

(17) Divakaruni, A. S.; Paradyse, A.; Ferrick, D. A.; Murphy, A. N.; Jastroch, M. Analysis and interpretation of microplate-based oxygen consumption and pH data. *Methods Enzymol* **2014**, *547*, 309−354. Pike Winer, L. S.; Wu, M. Rapid analysis of glycolytic and oxidative substrate flux of cancer cells in a microplate. *PLoS One* **2014**, *9* (10), No. e109916.

(18) Zhang, J.; Zhang, Q. Using Seahorse Machine to Measure OCR and ECAR in Cancer Cells. *Methods Mol. Biol.* **2019**, *1928*, 353−363. Plitzko, B.; Loesgen, S. Measurement of Oxygen Consumption Rate (OCR) and Extracellular Acidification Rate (ECAR) in Culture Cells for Assessment of the Energy Metabolism. *Bio Protoc* **2018**, *8* (10), No. e2850.

(19) Dowding, J. M.; Song, W.; Bossy, K.; Karakoti, A.; Kumar, A.; Kim, A.; Bossy, B.; Seal, S.; Ellisman, M. H.; Perkins, G.; et al. Cerium oxide nanoparticles protect against Abeta-induced mitochondrial fragmentation and neuronal cell death. *Cell Death Differ.* **2014**, *21* (10), 1622−1632.

(20) Li, X.; Qi, M.; Sun, X.; Weir, M. D.; Tay, F. R.; Oates, T. W.; Dong, B.; Zhou, Y.; Wang, L.; Xu, H. H. K. Surface treatments on titanium implants via nanostructured ceria for antibacterial and anti-inflammatory capabilities. *Acta Biomater* **2019**, *94*, 627−643.

(21) Yang, J.; Zhang, X.; Lu, B.; Mei, J.; Xu, L.; Zhang, X.; Su, Z.; Xu, W.; Fang, S.; Zhu, C.; et al. Inflammation-Responsive Hydrogel Spray for Synergistic Prevention of Traumatic Heterotopic Ossification via

https://doi.org/10.1021/acsomega.3c09025
ACS Omega 2024, 9, 21851−21863

Dual-Homeostatic Modulation Strategy. *Adv. Sci. (Weinh)* **2023**, *10*, No. e2302905.
(22) Higashikuni, Y.; Liu, W. H.; Numata, G.; Tanaka, K.; Fukuda, D.; Tanaka, Y.; Hirata, Y.; Imamura, T.; Takimoto, E.; Komuro, I.; et al. NLRP3 Inflammasome Activation Through Heart-Brain Interaction Initiates Cardiac Inflammation and Hypertrophy During Pressure Overload. *Circulation* **2023**, *147* (4), 338−355. Rong, W. W.; Liu, C. C.; Li, X. M.; Wan, N. F.; Wei, L. J.; Zhu, W. T.; Bai, P. Y.; Li, M.; Ou, Y. J.; Li, F.; et al. Caspase-8 Promotes Pulmonary Hypertension by Activating Macrophage-Associated Inflammation and IL-1β (Interleukin 1β) Production. *Arterioscl Throm Vas* **2022**, *42* (5), 613−631.
(23) Bogdanet, D.; Egan, A. M.; Reddin, C.; Kgosidialwa, O.; Kirwan, B.; Carmody, L.; Dunne, F. P. ATLANTIC DIP: Insulin Therapy for Women With IADPSG-Diagnosed Gestational Diabetes Mellitus. Does It Work? *J. Clin. Endocr. Metab.* **2017**, *102* (3), 849−857. Chen, B.; Du, Y. R.; Zhu, H.; Sun, M. L.; Wang, C.; Cheng, Y.; Pang, H.; Ding, G.; Gao, J.; Tan, Y.; et al. Maternal inheritance of glucose intolerance via oocyte TET3 insufficiency. *Nature* **2022**, *605* (7911), 761−766.
(24) Chen, H.; Ye, T.; Hu, F.; Chen, K.; Li, B.; Qiu, M.; Chen, Z.; Sun, Y.; Ye, W.; Wang, H.; et al. Urchin-like ceria nanoparticles for enhanced gene therapy of osteoarthritis. *Sci. Adv.* **2023**, *9* (24), No. eadf0988.

https://doi.org/10.1021/acsomega.3c09025
ACS Omega 2024, 9, 21851−21863